



# **JGR** Biogeosciences

# RESEARCH ARTICLE

10.1029/2022JG007048

#### **Key Points:**

- Patterns in carbon dioxide are almost entirely accounted for by instream metabolism except during a storm
- Methane is highly variable in space and covaries with aerobic respiration
- The stream shifts from a source of nitrous oxide to a sink during peak autumn respiration, likely due to nitrogen limitation

#### **Supporting Information:**

Supporting Information may be found in the online version of this article.

#### Correspondence to:

A. M. Carter, alice.m.carter@flbs.umt.edu

#### Citation:

Carter, A. M., DelVecchia, A. G., & Bernhardt, E. S. (2022). Patterns and drivers of dissolved gas concentrations and fluxes along a low gradient stream. *Journal of Geophysical Research: Biogeosciences*, *127*, e2022JG007048. https://doi.org/10.1029/2022JG007048

Received 16 AUG 2022 Accepted 3 NOV 2022

# **Author Contributions:**

Conceptualization: Alice M. Carter, Emily S. Bernhardt Data curation: Alice M. Carter Formal analysis: Alice M. Carter Funding acquisition: Emily S. Bernhardt Investigation: Alice M. Carter, Amanda G. DelVecchia

Methodology: Alice M. Carter, Amanda G. DelVecchia, Emily S. Bernhardt Project Administration: Alice M. Carter Resources: Emily S. Bernhardt Software: Alice M. Carter, Amanda G. DelVecchia

Supervision: Emily S. Bernhardt Visualization: Alice M. Carter, Amanda G. Del Vecchia, Emily S. Bernhardt Writing – original draft: Alice M. Carter

Writing – review & editing: Alice M. Carter, Amanda G. DelVecchia, Emily S. Bernhardt

© 2022. American Geophysical Union. All Rights Reserved.

# Patterns and Drivers of Dissolved Gas Concentrations and Fluxes Along a Low Gradient Stream

Alice M. Carter<sup>1,2</sup>, Amanda G. DelVecchia<sup>1,3</sup>, and Emily S. Bernhardt<sup>1</sup>

<sup>1</sup>Duke University, Durham, NC, USA, <sup>2</sup>Flathead Lake Biological Station, University of Montana, Missoula, MT, USA, <sup>3</sup>University of North Carolina, Chapel Hill, NC, USA

**Abstract** Freshwater ecosystems are globally significant sources of greenhouse gases (GHGs) to the atmosphere. Previous work has indicated that GHG flux in headwater streams is dominated by terrestrially derived gases, with in situ production limited by short organic matter residence times and high dissolved oxygen concentrations due to turbulent reaeration. However, low-gradient headwater streams that contain pool structures with longer residence times may be conducive to the in situ production of GHG. These streams, and the longitudinal heterogeneity therein, are seldom studied. We measured continuous ecosystem metabolism alongside concentrations and fluxes of carbon dioxide (CO<sub>2</sub>), methane (CH<sub>4</sub>), and nitrous oxide (N<sub>2</sub>O) in a low-gradient third order stream in the North Carolina Piedmont. From autumn to the following spring, we characterized spatial and temporal patterns of GHG along an 8 km segment in the context of channel geomorphology, hydrology, and ecosystem metabolic rates using linear mixed effects models. We found that stream metabolism was responsible for most of the CO<sub>2</sub> flux over this period, and that in-channel aerobic metabolism was a primary predictor of both CH<sub>4</sub> and N<sub>2</sub>O fluxes as well. Long water residence times, limited reaeration, and substantial organic matter from terrestrial inputs foster conditions conducive to the in-stream accumulation of CO<sub>2</sub> and CH<sub>4</sub> from microbial respiration. Streams like this one are common in landscapes with low topographic relief, making it likely that the high contribution of instream metabolism to GHG fluxes that we observed is a widespread yet understudied behavior of many small streams.

**Plain Language Summary** Stream ecosystems play a role in producing greenhouse gases (GHGs) and transporting them from groundwater to be released into the atmosphere. Some of these gases are produced through the breakdown of organic matter by microbes in the stream. We don't know how important this microbial production is compared to gases coming from soil and groundwater, but comparing it to rates of ecosystem metabolism may help us learn about it. We measured GHG and metabolism along a stream and found that metabolism is directly responsible for the production of carbon dioxide and is a good predictor of methane, meaning that microbial production in the stream is likely important.  $N_2O$  production was limited by competition between microbes for nitrogen, as a result, the stream was removing  $N_2O$  from the atmosphere rather than releasing it.

#### 1. Introduction

A significant fraction of the carbon fixed in terrestrial ecosystems is exported to streams as dissolved carbon dioxide ( $CO_2$ ), methane ( $CH_4$ ), dissolved organic matter, and particulate organic matter (Aufdenkampe et al., 2011). Rivers represent important landscape control points (sensu Bernhardt et al., 2017) by both actively mineralizing terrestrial organic matter and respiring it as  $CO_2$  and  $CH_4$  (Hotchkiss et al., 2015) and by transporting and degassing  $CO_2$  and  $CH_4$  from the terrestrial environment. Gaseous C emissions from freshwater ecosystems are increasingly recognized as an important component of regional and global carbon cycles, considerably offsetting estimates of terrestrial carbon sequestration (Battin et al., 2009; Holgerson & Raymond, 2016; J. Cole et al., 2007) and contributing to atmospheric forcing (Quick et al., 2019; Raymond et al., 2013).

Despite their importance for global climate forcing, estimates of GHG concentrations and fluxes in streams are still poorly constrained, in part due to high spatial and temporal variability. Many physical (Crawford et al., 2013; Lupon et al., 2019) and chemical (Schade et al., 2016) drivers have been shown to underly this variability, while studies that incorporate ecosystem metabolic cycling as a driver are less common (Crawford et al., 2014). It has been widely assumed that aquatic production of greenhouse gases (GHGs) is likely to be important only in large rivers (J. J. Cole & Caraco, 2001; Vannote et al., 1980) due to the higher connectivity of headwaters to terres-

CARTER ET AL. 1 of 17

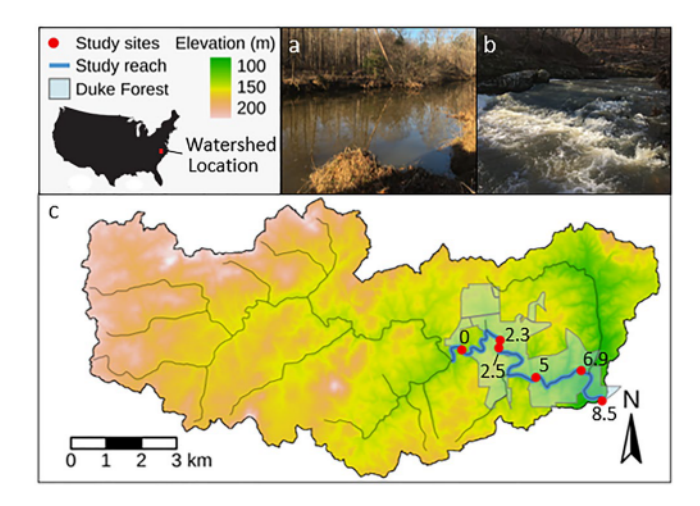


**Figure 1.** New Hope Creek watershed (35.980°N and -79.002°E) with photos of (a) a pool and (b) a run section taken on the same day in February 2019. (c) Topographic map of the watershed showing study sites as red points labeled with their km distances starting upstream. The watershed is mostly forested with the 8.5 km study reach contained entirely within the Duke Forest (outlined in gray).

trial gas inputs (Hotchkiss et al., 2015) and shorter processing time available for organic carbon in these systems (Catalán et al., 2016). However, recent studies have shown that mineralization of allochthonous organic matter can be a primary source of river GHG fluxes in some headwater streams as well (Bernal et al., 2022; Rocher-Ros et al., 2020), contributing to the high GHG fluxes observed in headwater streams (Li et al., 2021; Stanley et al., 2016).

While photosynthesis and aerobic respiration directly affect  $\mathrm{CO}_2$  concentrations, their control of oxygen concentrations may indirectly regulate the production of  $\mathrm{CH}_4$  and nitrous oxide ( $\mathrm{N}_2\mathrm{O}$ ) via anaerobic respiratory pathways (Megonigal et al., 2004). Positive relationships between aerobic respiration and  $\mathrm{CH}_4$  fluxes have been observed (Stanley et al., 2016) and may arise due either to a shared dependence on organic carbon substrates or to the indirect control of redox conditions by respiring aerobes.  $\mathrm{N}_2\mathrm{O}$  production in rivers has received far less attention but tends to be quite low, even for polluted rivers where rates of nitrification and denitrification are high (Beaulieu et al., 2011).

Climate change is altering the timing, magnitude, and spatial distribution of both terrestrial GHG delivery and aquatic GHG production in rivers. Changes in groundwater recharge are expected as a result of changing precipitation patterns and higher evapotranspiration in terrestrial ecosystems (Taylor et al., 2013). Decreased groundwater delivery at baseflow will likely reduce the magnitude of emissions derived from terrestrial sources and increase the

importance of riverine metabolism in driving GHG fluxes. In contrast, for rivers where climate change leads to flashier hydrology, riverine metabolic processes may be constrained by disturbance (Bernhardt et al., 2022), enhancing the relative importance of terrestrially derived GHGs (Blackburn & Stanley, 2021) and likely enhancing interannual variability in GHG concentrations and fluxes (Junker et al., 2020). In all rivers, warming temperatures may drive higher rates of in stream carbon processing (Yvon-Durocher et al., 2010) and the production of CO<sub>2</sub> and CH<sub>4</sub> (Demars et al., 2016; Yvon-Durocher et al., 2014), pushing the carbon balance in streams toward faster mineralization and reduced storage and transport.

We measured oxygen and GHG concentrations along an eight km segment of New Hope Creek in the North Carolina Piedmont. This site is a heterotrophic, low-gradient stream with a forested catchment. Rates of instream gross primary productivity (GPP) are highest from late winter until the canopy closes in April, while rates of ecosystem respiration (ER) peak following litterfall in October (Carter, 2021; C. A. S. Hall, 1972). To capture both periods of peak instream metabolic activity our study extended from the end of autumn through the productivity peak in the following spring. Over the course of these three seasons, we measured dissolved oxygen concentrations continuously and calculated daily rates of stream GPP and ER at six sites for each date on which we collected gas concentration and gas flux measurements. We examined the relationship between gas dynamics and physical and biogeochemical drivers using linear mixed effects models and gas ratios. Our goals were to (a) characterize the patterns and magnitudes of GHG concentrations and fluxes, (b) determine potential drivers of gas dynamics, and (c) describe the role of in stream processing in generating and consuming GHGs in New Hope Creek through space and time.

#### 2. Methods

#### 2.1. Site Description

The New Hope Creek watershed is located in the North Carolina Piedmont within Durham and Orange Counties, NC at 36°N, -79°E. In the 8.5 km stream section in this study, New Hope Creek is a third order stream and flows through a fully forested section of the Duke Forest (Figure 1). The study watershed (delineated to the outlet of our study reach, see below) is 81 km² with 90% forest cover, 9% agricultural land, and 1.3% developed land based on 2016 NLCD data (Carter, 2021). The study reach has an average depth of 0.4 m and width of 14.4 m measured in March and an average slope of 3.2 m km<sup>-1</sup>. Along this section, New Hope Creek is in the Triassic basin and the stream alternates between long deep pools and short bedrock outcrops that create riffles (Figure 1). Even during

CARTER ET AL. 2 of 17

periods of steady flow, there is no measurable water velocity in the large pools and water residence times last from hours up to several days. Seasonally, discharge varies several orders of magnitude between high flow storm peaks throughout the winter and spring, and frequent, extended dry periods in autumn. This study was initiated when flow resumed, after a period of no flow in October when the creek had become a series of disconnected pools. During our study from November 2019 to March 2020 there was constant stream flow with a median of 0.7 m<sup>3</sup> s<sup>-1</sup> at the outlet.

Our six monitoring sites spanned an 8.5 km reach starting at the most upstream site at 0 km (NHC\_0) to the outlet of our reach at the downstream point NHC\_8.5. All sites are named based on their distance in km from the top to the bottom of the reach. Two of the sites are in long deep pools: NHC\_2.3 (2,330 m) and NHC\_6.9 (6,880 m). Three sites are in shorter pools that often transitioned to runs: NHC\_0 (0 m), NHC\_5 (5,000 m), and NHC\_8.5 (8,450 m). One site is in a run downstream of a riffle: NHC\_2.5 (2,500 m), Figure 1. We measured the distance to each of these sites starting at 8.5 km and walking up the stream channel with a hip chain (Forestry Supply) counting distance in meters. We measured the latitude and longitude of each site using a handheld GPS and paired them with reaches in the National Hydrography Dataset (U.S. Geological Survey, 2017) using the nhdplusTools package (Blodgett, 2019) in R (R Core Team, v. 3.6.3) to obtain the contributing watershed area for each site.

#### 2.2. Sensor Deployment

At each of our monitoring locations, we collected continuous measurements of dissolved oxygen concentrations and temperature (Onset HOBO U26, Bourne, MA, USA), and water pressure (Onset HOBO U20L) at 15-min intervals from November 2019 to March 2020. We deployed sensors attached to a fence post at all sites except for NHC\_8.5, which was mounted directly to bedrock, in the thalweg of the stream or one m from the side of the stream in deep pool sites (NHC\_7 and NHC\_2.3). The sensors were mounted inside of a 3" PVC pipe with many 1" holes drilled to allow for complete water flow. These PVC cages were placed so that the sensors were measuring at ~25 cm below the surface during average baseflow. We calibrated the dissolved oxygen sensors in the lab prior to deployment by placing them in 100% air saturated water to set 100% saturation point. To do this, bubbled a bucket of water with ~20 L of room temperature water with air forced through a ceramic aquaculture stone for 1 hr then allowed the bucket to equilibrate for 10 min to avoid measuring supersaturated water (Blaszczak et al., 2019). For a 0% saturation point, we placed the sensors in a 1M sodium sulfite solution until they equilibrated. We deployed dissolved oxygen sensors with copper antibiofouling caps. During the deployment period, we visited the sensors at least biweekly to clear debris and clean biofilms from the sensor and PVC housing with a brush and to download data.

#### 2.3. Hydrology and Channel Morphology

We modeled discharge at the upstream (NHC\_0) and downstream (NHC\_8.5) monitoring sites based on continuous water level data collected by pressure transducers. Over a range of flow conditions, we measured stream discharge by velocity profiling with an electromagnetic sensor (Marsh-McBirney Flo-Mate, Frederick, MD, USA) and built site specific level-discharge rating curves based on measurements at NHC\_0 (n = 11) and NHC\_8.5 (n = 13) with a bank-full high flow point added at each site by calculating flow based on Manning's equation for open channel flow. To estimate discharge at the intervening sites, we assumed that flow accumulation was proportional to accumulated upslope area (Leach et al., 2017) during periods when the stream was gaining flow and that flow loss was proportional to stream length during periods of losing flow and calculated discharge by interpolating the continuous measurements from sites NHC\_0 and NHC\_8.5. Flow did not exceed the maximum points on our discharge rating curves for any of our GHG sampling dates.

We estimated the total groundwater flux along the study reach on each of our sampling dates using the discharge measurements from NHC\_0 and NHC\_8.5. To do this, we calculated the total groundwater contribution as the change in discharge (aggregated to a daily time step for each sampling date) from the top to the bottom of the study reach. We divided this rate by the stream bed area (calculated with the channel width measurements below) to calculate a groundwater flux in  $m^3 m^{-2} d^{-1}$ . We present the distribution of groundwater fluxes on our sampling dates in the supplementary information (Figure S1 in Supporting Information S1).

We conducted channel morphology surveys in the 1 km reaches upstream of NHC\_0 and NHC\_8.5 by measuring cross-sections of depth, channel width, and stream bank heights every 100 m for a total of 10 locations at

CARTER ET AL. 3 of 17

each site. We followed the streamPULSE geomorphic survey protocol (streampulse.org) to collect these measurements. From these 20 cross sections, we developed a linear relationship between thalweg depth and average channel depth. We conducted two separate surveys of the entire 8.5 km study reach measuring channel width and thalweg depth every 50 m at high flow (9 March 2019) and at low flow (8 October 2019). We converted thalweg depths to average depth according to our empirical relationship and used this data to calculate average depth in the 1 km reach above each sensor site at two separate time points (Carter, 2021). We paired these depth measurements with discharge estimates calculated for each site on the respective days and used this pair of points to calculate site specific parameters for this empirical depth (D) by discharge (Q) relationship (Leopold & Maddock, 1953):

$$D = cQ^f \tag{1}$$

where c is the average depth at unit discharge and f is a unitless coefficient.

At each sensor location, we calculated stream bed slope from a 30-m resolution LiDAR map of the study water-shed available through the North Carolina State University Libraries (https://www.lib.ncsu.edu/gis/elevation). We used the continuous\_stream\_slope function in the whiteboxTools package (Lindsay, 2014) in R (v 3.6.3) to extract stream slopes from the LiDAR images.

#### 2.4. Water Chemistry Analyses

We measured dissolved ions, dissolved organic carbon (DOC), and dissolved gas concentrations on 11 different dates from 11 November 2019 to 21 March 2020 at intervals ranging from 1 to 3 weeks. At each sample date, we collected a water sample for laboratory analyses from all six monitoring locations. We measured water temperature, conductivity, pH, and dissolved oxygen and atmospheric pressure at the time of sample collection with a handheld meter (Yellow Springs Instruments, Columbus, OH, USA). We collected water from  $\sim$ 15 cm below the surface and filtered it through ashed 25 mm GF/F filters into acid washed HDPE 60 mL bottles. We kept water samples on ice until they could be frozen at -20 C until analysis. We analyzed the water samples for nitrate (NO<sub>3</sub>-N) on a Dionex ion chromatograph (ICS-2000) with a KOH eluent generator and an IonPac AS-18 analytical column (Dionex Corporation, Sunnyvale, CA, USA). The minimum detection limit (mdl) for NO<sub>3</sub> was 5 µg N L<sup>-1</sup>, seven samples were below detection and these were set to 2.5 µg N L<sup>-1</sup>. We analyzed total dissolved nitrogen (mdl = 0.05 mg L<sup>-1</sup>) and DOC (mdl = 0.25 mg L<sup>-1</sup>) on a Shimadzu TOC-V total carbon analyzer that had a TNM-1 nitrogen module (Shimadzu Scientific Instruments, Colombia, MD, USA).

# 2.5. Dissolved Gas

We collected dissolved gas samples in duplicate alongside each water sample and used laboratory headspace equilibration to obtain a gas sample for analysis (adapted from Hudson (2004)). We used preweighed, 60-mL crimp-capped glass serum vials that were evacuated in the laboratory no more than 24 hr in advance of sampling. In the field, we collected a water sample by placing the evacuated vial 5-10 cm below the surface of the water, inserting a 20 gauge needle and allowing the vial to fill to ~40 mL before removing the needle below the water surface. On multiple sample days, we also collected atmospheric samples in evacuated 9 mL glass serum vials at the sample sites. Samples were stored on ice in the dark for no more than 2 hr between collection and headspace equilibration, consistent with NEON protocols for dissolved GHG sample collection (Goodman, 2021). We determined the volume of each sample by weight with a Mettler Toledo PB precision balance (0.01 g). To equilibrate samples, we added N<sub>2</sub> gas with a glass syringe to the evacuated headspace until vials were at atmospheric pressure, then added an additional 15 mL of N<sub>2</sub> to overpressurize the headspace. We then placed the vials on a shaker table for 2 min to allow the dissolved gases to equilibrate with the nitrogen headspace. After shaking, we transferred 10 mL of headspace from each sample into an evacuated 9-mL glass serum vial using a glass syringe. We then immediately uncapped the samples and measured water temperature and lab air pressure for equilibration calculations. On the day of equilibration, we prepared a five point standard curve in triplicate in evacuated 9 mL serum vials that we stored with the samples until analysis, always within 2 weeks of sample collection. Hold time tests for both the serum bottle samples (<2 hr) and the gas vials (<2 weeks) indicate minimal effects on concentration.

We analyzed gas samples for carbon dioxide  $(CO_2)$ , methane  $(CH_4)$ , and nitrous oxide  $(N_2O)$  in the extracted headspace within 2 weeks of collection. We conducted our analyses with a Shimadzu 17A gas chromatograph

CARTER ET AL. 4 of 17

equipped with an electron capture detector (ECD) and a flame ionization detector (Shimadzu Scientific Instruments, Colombia, MD). To allow for determination of multiple gas concentration from the same sample, we attached sixport valves and a methanizer. Duplicate samples were injected with a Tekmar 7050 Headspace Autosampler and run with ultrahigh purity  $N_2$  as the carrier gas and a P5 mixture as the make-up gas for the ECD. Medical grade breathing air was plumbed through a Nafion tube to remove water vapor from the sample stream. We used a five point standard curve of known concentrations (certified primary standards, Airgas, Morrisville, NC, USA) to convert peak areas of samples into gas concentrations.

We calculated the dissolved gas concentration in the water sample based on the headspace concentration (see below for analysis) following Hudson, 2004. First, we calculated the aqueous concentration of the gas that was partitioned into the headspace during equilibration ( $C_{\Delta H}$ ).

$$C_{\rm AH} = \frac{V_h}{V_w} \times C_g \times \rho_g \tag{2}$$

where  $V_h$  is the volume of  $N_2$  in the headspace and  $V_w$  is the volume of water,  $C_g$  is the measured gas concentration in mL mL<sup>-1</sup>, and  $\rho_g$  is the density of the gas (mg L<sup>-1</sup>). We then calculated the concentration of gas still in the aqueous phase after equilibration ( $C_A$ ) using gas specific Henry's Law constants (H, atm mol<sup>-1</sup> fraction):

$$C_A = \frac{p_g}{H} \times \frac{n_w}{V_w} \times MW_g \tag{3}$$

where  $p_g$  is the partial pressure of the gas at lab atmospheric pressure,  $n_w/V_w$  is the molar concentration of water (55.5 mol L<sup>-1</sup>), and  $MW_g$  is the molecular weight of the gas (mg L<sup>-1</sup>). The total concentration of gas in the water sample (C, mg L<sup>-1</sup>) is as follows:

$$C = C_{AH} + C_A \tag{4}$$

#### 2.6. Gas Flux

We estimated gas fluxes to the atmosphere  $(F, \text{ mg m}^{-2} \text{ d}^{-1})$  for each sample using the following equation:

$$F = (C - C_{\text{sat}}) \times k_g \tag{5}$$

where C (mg L<sup>-1</sup>) is the dissolved gas concentration in the water,  $C_{\rm sat}$  (mg L<sup>-1</sup>) is the saturation concentration of the gas at equilibrium with the atmosphere (calculated using Henry's law), and  $k_g$  (m d<sup>-1</sup>) is the gas exchange velocity for a specific gas (Raymond et al., 2012). The geomorphology in New Hope Creek is dominated by long deep pools where average water velocities are low, even during moderate flow when water volume is high (~0.1 m s<sup>-1</sup> at 1 m<sup>3</sup> s<sup>-1</sup>) resulting in low gas exchange velocities and long turnover distances for dissolved gases. Because of this, open channel methods for measuring gas exchange with a tracer gas (R. O. Hall & Madinger, 2018) do not produce reliable results. We therefore estimated gas exchange coefficients using inverse modeling based on dissolved oxygen time series (R. O. Hall & Ulseth, 2020). From the model (see Metabolism section for details), we generated a pooled relationship between  $K_{600}$  (gas exchange coefficient in d<sup>-1</sup>, normalized to a Schmidt number of 600) and discharge at each site, which we used to calculate a daily  $K_{600}$  value (Appling, Hall, Yackulic, & Arroita, 2018; Figure S3 in Supporting Information S1). We converted our model derived estimates of  $K_{600}$  (d<sup>-1</sup>) to  $k_{600}$  (m d<sup>-1</sup>) multiplying by average stream depth and then calculated gas specific values ( $k_g$ , m d<sup>-1</sup>):

$$k_g = \left(\frac{\text{Sc}_g}{600}\right)^{(-1/2)} / k_{600} \tag{6}$$

using the gas specific Schmidt numbers ( $Sc_g$ ) calculated at the sample water temperature according to the coefficients in Raymond et al., 2012.

We used the depth-normalized  $K_g$  (d<sup>-1</sup>) values for each gas along with average velocity ( $\nu$ , m d<sup>-1</sup>) to estimate the turnover 95% length of the gas as ~3  $\nu/K_g$  (Chapra & Di Toro, 1991). These estimates were almost always greater than our 1 km "footprints" upstream of each sensor site.

CARTER ET AL. 5 of 17

#### 2.7. Metabolism

We modeled metabolism based on the single station diel  $O_2$  method using the hierarchical Bayesian state space model StreamMetabolizer (Appling, Hall, Arroita, & Yackulic, 2018) in R (v. 3.6.3). This model estimates daily rates of GPP, ER, and the gas exchange coefficient  $K_{600}$  based on changes in oxygen concentration over time according to the following equation:

$$\frac{dO_2}{dt} = GPP_t + ER_t + k_{O_2} \times (DO_t - DO_{sat,i})$$
(7

where  $k_{\rm O2}$  (m d<sup>-1</sup>) is the oxygen specific gas exchange coefficient related to  $K_{600}$  by the Schmidt number for  $O_2$  (Equation 6),  $DO_i$  and  $DO_{\rm sat,i}$  are the instantaneous concentration of dissolved oxygen and the concentration at saturation in the stream, and  $GPP_i$ ,  $ER_i$  are daily, volumetric rates (g  $O_2$  m<sup>-3</sup> d<sup>-1</sup>). We used a model with both observation and process error and with partial pooling of  $K_{600}$ , which restricts the amount of variation allowed in the  $K_{600}$  by discharge relationship to reduce equifinality in model solutions (Appling, Hall, Yackulic, & Arroita, 2018). We ran the model with uninformative priors on GPP and ER and with a weak prior on  $K_{600}$  with a mean calculated based on empirical relationships for headwater streams (Raymond et al., 2012) and a standard deviation of 0.7 at each node in the K-Q relationship (for more details on model fitting of our data, see Carter, 2021). After estimating metabolism, we removed model estimates for which the  $R_{\rm hat}$ , a metric of parameter convergence, was above 1.05 or for which ER was greater than zero or GPP less than zero with a 95% CI that did not contain zero. See Supporting Information S1 for plots of sensor data used to estimate metabolism (Figure S2 in Supporting Information S1) and evaluation of model K-Q and K-ER relationships (Figure S3 in Supporting Information S1).

#### 2.8. Data Analysis

To determine how gas concentrations and fluxes varied along with hypothesized physical and biological drivers, we fit the following models:

$$y_{i,j} = \beta X_{i,j} + u_i + v_j + \varepsilon_{i,j}$$

$$u_i \sim N(0, \sigma_{\text{meas}}^2)$$

$$v_j \sim N(0, \sigma_{\text{site}}^2)$$

$$\varepsilon_{i,j} \sim N(0, \sigma_{\text{proc}}^2)$$
(8)

where  $y_{i,j}$  is the gas concentration or flux for the *i*th sample at the *j*th site,  $\beta$  is a vector of coefficients, and  $X_{i,j}$  is a vector of measured covariates  $(1, x_1, ..., x_n)_{i,j}$  for each sample and site. Residual variation is partitioned into measurement error (variation between replicates:  $u_i$ ) and process error which includes unexplained variation between sites  $(v_j)$  and unexplained residual variation  $(\varepsilon_{i,j})$ . We performed model selection in R (v 4.1.3, R Core Team, 2022) with the lme4 package (Bates et al., 2015) using the code lmer(y ~ (1|rep) + (1|site) + x1 + ... + x n) on z-scored data and predictors. Each baseline model contained a random intercept for sample replicate, subsequent models added a random intercept for site and different combinations of stream geomorphic characteristics (stream slope and average depth), physical properties (water temperature and discharge), stream metabolism (GPP and ER), and water chemistry (concentration of  $NO_3^-$ , DOC, and  $O_2$ ).

We conducted model selection based on Akaike's Information Criterion corrected for small sample sizes (Hurvich & Tsai, 1989) and restricted possible models to those that contained five or fewer fixed effects and did not allow inclusion of both discharge and DOC, which are highly correlated (r = 0.82, p < 0.001). All other predictors have r < 0.6, but to prevent multicollinearity, we only considered models with variance inflation factors of less than 5 (Beier et al., 2001). Nitrate was only included in models for N<sub>2</sub>O concentration and flux. Average depth was included in models for gas concentrations but not fluxes as depth was used directly in the calculations of gas flux. We present the top five models for each gas in Table S1 in Supporting Information S1 and the single best models in Tables 1 and 2. For the best fit models, we calculated a marginal R<sup>2</sup>, which describes the variance explained by just the fixed effects ( $x_1, \ldots, x_n$ ) and a conditional R<sup>2</sup>, which is the variance explained by the whole model including random intercepts (Nakagawa & Schielzeth, 2013).

CARTER ET AL. 6 of 17

| Model            |      | w <sub>AICc</sub> (%) | R <sup>2</sup> m | R <sup>2</sup> c | VIF  | Model predictors                          |
|------------------|------|-----------------------|------------------|------------------|------|---|
| CO <sub>2</sub>  | Conc | 59                    | 0.797            | 0.980            | 1.98 | Site + Temp + GPP + $O_2$                 |
|                  | Flux | 48                    | 0.661            | 0.970            | 1.60 | $\log(Q) + \text{GPP} + \text{O}_2$       |
| CH <sub>4</sub>  | Conc | 45                    | 0.757            | 0.948            | 1.66 | Slope + $log(Q)$ + GPP + $O_2$            |
|                  | Flux | 60                    | 0.553            | 0.871            | 1.64 | Slope + Temp + $GPP + ER$                 |
| N <sub>2</sub> O | Conc | 38                    | 0.489            | 0.866            | 1.24 | $\log(Q) + \text{ER} + \log(\text{NO}_3)$ |
|                  | Flux | 46                    | 0.463            | 0.850            | 1.65 | $ER + O_2 + \log(DOC) + \log(NO_3)$       |

*Note.* All models include a random intercept for sample replicate in addition to the listed predictors. Best model was selected based on Akaike's Information Criterion (AICc; see Table S1 in Supporting Information S1).  $w_{AICc}$ : Model weight out of top five models,  $R^2$ m: Marginal  $R^2$  (fit of fixed effects),  $R^2$ c: Conditional  $R^2$  (fit including random effects), VIF: variance inflation factor. See text for details.

To further evaluate the links between GHGs and stream metabolism, we calculated the fraction of  $O_2$  and  $CO_2$  flux that could be explained by gas production or consumption due to net ecosystem metabolism (net ecosystem production, NEP = GPP – ER). We converted oxygen based metabolism estimates to units of  $CO_2$  using a respiratory quotient (RQ) of 0.8 measured as moles of  $CO_2$  produced per mole of  $O_2$  consumed (del Giorgio & Peters, 1994). We used the reciprocal of this (1.25) as a photosynthetic quotient. We calculated the fraction of instream contribution as NEP  $_g/F_g$  (the gas specific NEP rate divided by the gas flux rate). If this fraction was larger than one (n = 14), we considered that to be 100% contribution. If this fraction was negative (i.e., gas flux to the atmosphere and gas consumption by NEP, n = 15), we considered that to be 0% contribution.

For oxygen,  $CO_2$ , and  $CH_4$ , we calculated the gas departure from atmospheric equilibrium for each sample. This is the amount of dissolved gas in excess of the saturation concentration, or the saturation deficit if the gas is undersaturated. We calculated gas specific saturation concentrations based on temperature and the atmospheric partial pressure using Henry's Law. The gas departure represents a source (e.g., groundwater and production) or a sink (e.g., consumption and oxidation) of the gas other than exchange with the atmosphere (Vachon et al., 2020). We present the molar ratios of  $CO_2:O_2$  departures and  $CH_4:CO_2$  departures and discuss various biogeochemical processes in the context of these ratios.

To see if the respiration and atmospheric CO<sub>2</sub> fluxes we observe could be accounted for by the DOC in the stream, we calculated DOC uptake rates. Based on a literature value for reach-scale DOC uptake velocity  $(v_f)$  of 0.26 mm min<sup>-1</sup> (Mineau et al., 2016), we estimated DOC uptake  $(U, \text{ mg m}^{-2} \text{ d}^{-1})$  based on our measured DOC concentrations:  $U = v_f \times [\text{DOC}]$ .

| Table 2  |  |
|--|--|
| Model Estimates and Uncertainties for Each of the Top Models |  |

| Model            |      | Slope   | $Q^{\mathrm{a}}$ | Temp    | ER      | GPP     | $O_2$   | DOCa    | NO <sub>3</sub> <sup>a</sup> | $\sigma_{ m site}^2$ | $\sigma_{ m proc}^2$ | $\sigma_{ m meas}^2$ |
|------------------|------|---------|------------------|---------|---------|---------|---------|---------|------------------------------|----------------------|----------------------|----------------------|
| CO <sub>2</sub>  | Conc | -       | -                | -0.55** | -       | -0.21*  | -0.81** | -       | -                            | 0.056                | 0.127                | 0.020                |
|                  | Flux | -       | 0.59**           | -       | -       | -0.23*  | -0.44** | -       | _                            |                      | 0.311                | 0.030                |
| CH <sub>4</sub>  | Conc | -0.36** | -0.45**          | -       | -       | -0.32** | -0.54** | -       | -                            |                      | 0.193                | 0.053                |
|                  | Flux | -0.42** | -                | 0.40**  | 0.45**  | -0.57** | -       | -       | -                            |                      | 0.329                | 0.134                |
| N <sub>2</sub> O | Conc | -       | -0.42**          | -       | -0.35** | -       | -       | -       | 0.59**                       |                      | 0.386                | 0.137                |
|                  | Flux | -       | -                | -       | -0.67** | -       | -0.49** | -0.37** | 0.53**                       |                      | 0.400                | 0.155                |

*Note.* Model estimates are given for each selected predictor with \* and \*\* indicating significance at the 0.01 and 0.001 levels, respectively. Standard deviations of random intercepts are shown for between sites ( $\sigma^2_{\text{site}}$ ), between replicates ( $\sigma^2_{\text{meas}}$ ) and residual unexplained variation attributed to process error ( $\sigma^2_{\text{proc}}$ ). All values are based on *z*-scored data.

<sup>a</sup>Discharge (Q), dissolved organic carbon (DOC), and nitrate (NO₃) are all on a log scale.

CARTER ET AL. 7 of 17

elibrary.wiley.com/doi/10.1029/2022JG007048 by University Of Wyoming Librarie, Wiley Online Library on [29/05/2023]. See the Terms

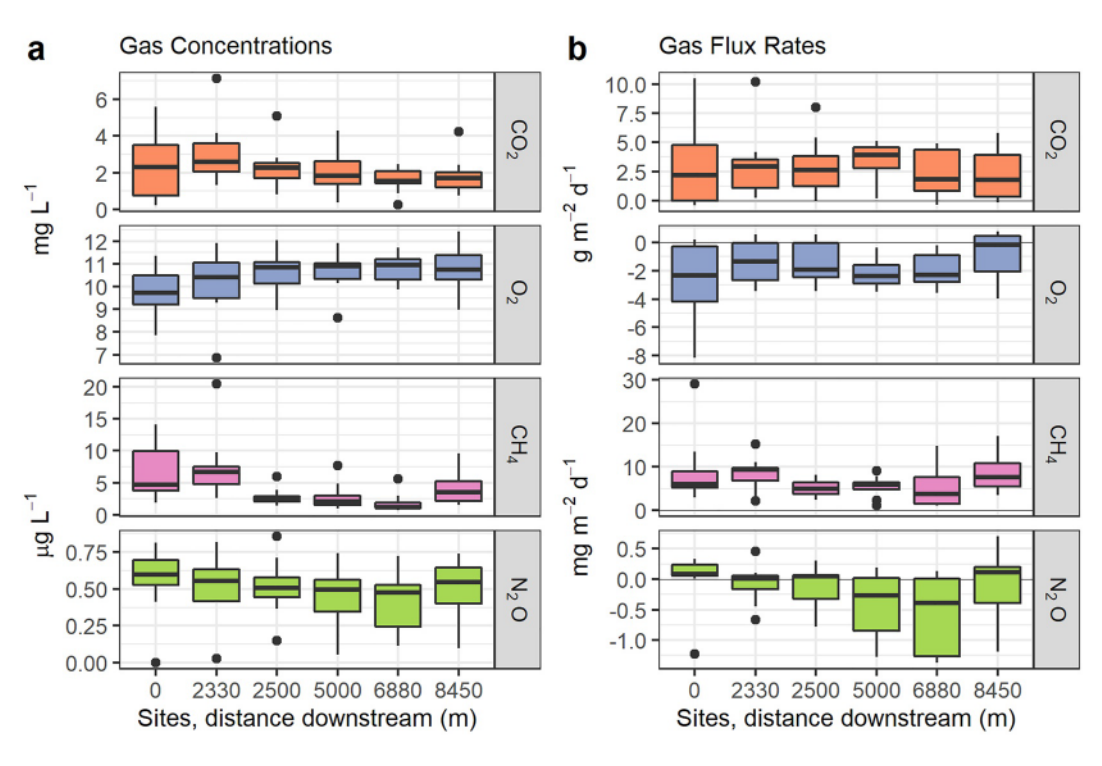


Figure 2. Longitudinal variation in dissolved gas (a) concentrations and (b) fluxes at each of the six study sites. Box plots show the distributions across all sample dates (n = 11).

#### 3. Results

# 3.1. Gas Concentrations and Fluxes

We measured dissolved gas concentrations at six sites on dates spanning November to March for a total of 58 site by date combinations. The concentration of oxygen  $(O_2)$  ranged from 6.9 to 12.4 mg L<sup>-1</sup> (mean  $\pm$  SD:  $10.5 \pm 1.1$  mg L<sup>-1</sup>), carbon dioxide (CO<sub>2</sub>) ranged from 0.2 to 7.1 mg L<sup>-1</sup> (2.3  $\pm$  1.4 mg L<sup>-1</sup>), methane (CH<sub>4</sub>) ranged from 0.7 to 20.5 µg L<sup>-1</sup> (4.3  $\pm$  3.4 µg L<sup>-1</sup>), and nitrous oxide (N<sub>2</sub>O) ranged from 0 to 0.86 µg L<sup>-1</sup> (0.48  $\pm$  0.21 µg L<sup>-1</sup>). Gas exchange coefficients were typically low ( $K_{600} = 7 \pm 4$  d<sup>-1</sup>, but up to 20 on a high flow sample day), resulting in low gas fluxes. On average, oxygen was undersaturated and was dissolving from the atmosphere ( $-1.8 \pm 1.7$  g m<sup>-2</sup> d<sup>-1</sup>). The stream was nearly always effluxing CO<sub>2</sub> (2.9  $\pm$  2.5 g m<sup>-2</sup> d<sup>-1</sup>) and CH<sub>4</sub> (6.9  $\pm$  4.7 mg m<sup>-2</sup> d<sup>-1</sup>), while N<sub>2</sub>O switched from undersaturated to supersaturated during the study with fluxes ranging from -1.4 to 0.71 mg m<sup>-2</sup> d<sup>-1</sup> ( $-0.22 \pm 0.52$  mg m<sup>-2</sup> d<sup>-1</sup>, Figure 2). While there were some consistent patterns of increasing or decreasing concentrations between sites, when averaged across all sample dates only CH<sub>4</sub> concentration was significantly different across sites (F = 5.2, p = 0.0006). Gas fluxes did not differ significantly across sites for any gas (Figure 2).

There was more variation in gas concentrations and fluxes over time than over space (Figure 3). From November to March, each dissolved gas showed a different pattern. Dissolved oxygen was low in November, (8.8  $\pm$  1.4 mg  $L^{-1}$ , mean  $\pm$  SD across sites on a single sample date) and increased throughout the winter, peaking in late January (11.8  $\pm$  0.4 mg  $L^{-1}$ ). CO $_2$  started at its highest point in November (5.2  $\pm$  1.2 mg  $L^{-1}$ ) and decreased through March to a minimum of 0.6  $\pm$  0.4 mg  $L^{-1}$ . CH $_4$  also had its peak in November (11  $\pm$  6.4 µg  $L^{-1}$ ) then decreased to a February low of 1.5  $\pm$  0.7 µg  $L^{-1}$  before rising in the spring to 7.5  $\pm$  2 µg  $L^{-1}$  by the end of March. N $_2$ O did not have consistent temporal trends; concentration was at its minimum in mid-November (0.07  $\pm$  0.06 µg  $L^{-1}$ ), its maximum in late January (0.78  $\pm$  0.05 µg  $L^{-1}$ ) and is the most variable in early December (Figure 3). Gas fluxes show similar patterns to their concentrations with the exception that N $_2$ O switches from being absorbed by the stream from November to mid-January to degassing from the stream for the remainder of the spring.

Best fit linear mixed effects models explained 80%, 76%, and 49% of the variation in CO<sub>2</sub>, CH<sub>4</sub>, and N<sub>2</sub>O concentrations and 66%, 55%, and 46% of the variation in fluxes, respectively, based on variation in fixed effects.

CARTER ET AL. 8 of 17

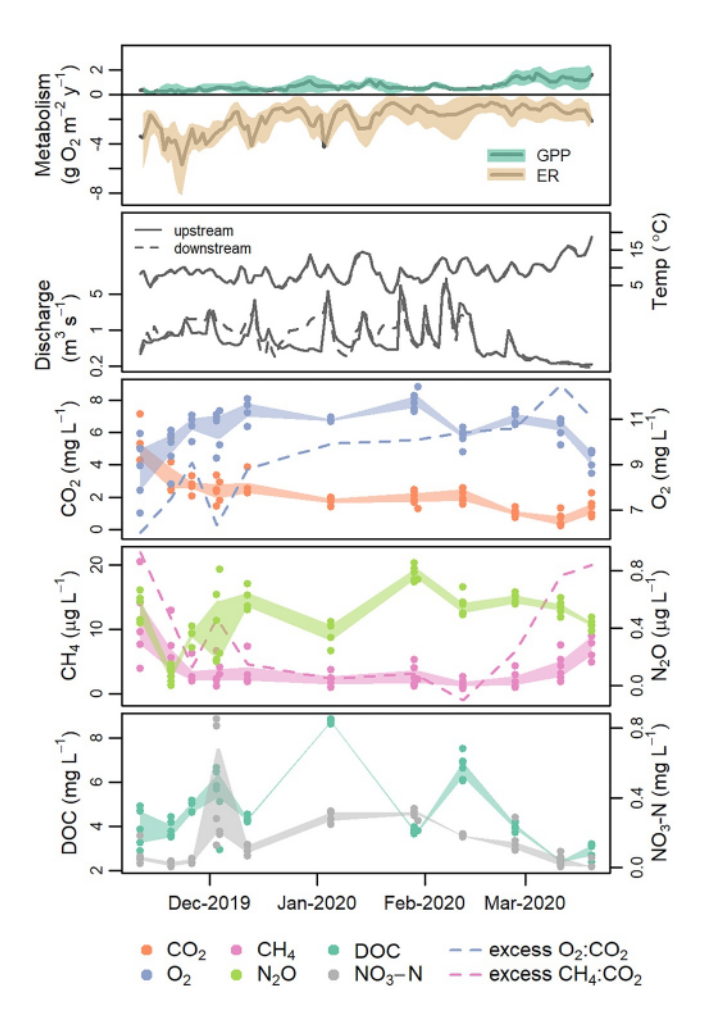


Figure 3. Temporal patterns in stream gas concentrations, physical and metabolic drivers in New Hope Creek. From top to bottom: mean daily gross primary productivity (GPP) and ecosystem respiration (ER) shown with 95% CIs; mean daily water temperature and discharge (Q) at the upstream (0 m) and downstream (8,450 m) sites; gas concentrations and water chemistry with samples from each site shown as points and shaded interquartile ranges. Dashed lines on the gas panels represent unitless ratios of gas concentrations in excess of saturation.

Variation across sites helped predict  $\mathrm{CO}_2$  concentration with unmeasured site characteristics explaining  $\sim\!6\%$  of unmodeled variability as a random effect. For  $\mathrm{CH}_4$  concentration and flux, the slope of stream sites was a better predictor than site alone, with steeper stream beds predicting less  $\mathrm{CH}_4$ . Stream discharge varied by over an order of magnitude between sampling dates (Figure 4) with low flows predicting low  $\mathrm{CH}_4$  and  $\mathrm{N}_2\mathrm{O}$  concentrations. Because of the strong positive correlation between discharge and DOC, we consider the relevance of both predictors when one was selected, suggesting that  $\mathrm{N}_2\mathrm{O}$  fluxes may also decrease with higher flows.

Stream metabolism was selected as a predictor in every model (Table 1). More primary productivity (GPP) predicted lower concentrations and fluxes of CO2 and CH4. More respiration (ER) predicted lower concentration and flux of N<sub>2</sub>O. While ER was not selected as a predictor for CO<sub>2</sub> or CH<sub>4</sub>, less oxygen, which is correlated with higher ER (Figure 4), predicts more of both gases. Interestingly, N<sub>2</sub>O flux is negatively predicted by both ER and O<sub>2</sub>, despite their negative covariance, suggesting that they reflected independent controls. Finally, variation in water chemistry significantly predicts N<sub>2</sub>O with more nitrate predicting higher concentrations and fluxes and more DOC predicting lower N2O. In the fall, when nitrate concentrations are the lowest, N<sub>2</sub>O is undersaturated and fluxes are negative (Figure S5 in Supporting Information S1) indicating that nitrate may be limiting production. Considering discharge as a proxy for DOC may suggest that higher DOC is linked to higher  $CO_2$  and lower  $CH_4$ . Across all models, measurement error ( $\sigma^2_{meas}$ ) accounted for ~15% (0.15 SD) of the unmodeled variability in CO2, 18% (0.27 SD) in CH<sub>4</sub>, and 29% (0.38 SD) in N<sub>2</sub>O (Table 2).

# 3.2. Gas Dynamics and Metabolism

In stream production of  $CO_2$  by aerobic respiration contributed substantially to the total flux of  $CO_2$ . We calculated rates of  $CO_2$  production from NEP assuming a RQ of 0.8 mol  $CO_2$  produced per mol  $O_2$  consumed. In-stream NEP was negative on 117 of 131 days, and for clarity we refer to this excess of respiration over photosynthetic assimilation as net heterotrophy (sensu C. A. S. Hall, 1972). Of the cumulative 161 g  $CO_2$  m<sup>-2</sup> effluxed from the stream across all sampling dates and locations, 64% can be accounted for by net heterotrophy. Across sampling days, the net heterotrophic contribution to  $CO_2$  efflux spanned the full range from 0% (NEP  $\geq$  0 or  $CO_2$  flux  $\leq$  0) to 100% (Net heterotrophy  $\geq$   $CO_2$  flux). In autumn, when litter inputs and high temperatures stimulated high rates of ER, net heterotrophy accounted

for  $78\% \pm 20\%$  of the  $CO_2$  flux. In the spring, when fluxes of photosynthesis were highest and sometimes exceeding fluxes of ER, net heterotrophy accounted for only  $27\% \pm 40\%$  of the  $CO_2$  flux. We measured the lowest net contribution of heterotrophy to total  $CO_2$  fluxes in our late February sampling ( $17\% \pm 40\%$ ), which took place on the falling limb of a large storm (Figure 5). These findings are robust to variations in the RQ ranging from 0.6 to 1 (Figure S6 in Supporting Information S1).

Groundwater fluxes through the stream bed approximated based on change in discharge along the entire 8.5 km reach was on average  $-0.04 \text{ m}^3 \text{ m}^{-2} \text{ d}^{-1}$  across all sample dates (Figure S1 in Supporting Information S1). On seven out of the 11 sample dates, the groundwater flux was negative, meaning the stream was losing water along the reach. Three sample dates from late November to early December had positive groundwater fluxes with the stream gaining at rates of 0.17, 0.40, and 0.19 m<sup>3</sup> m<sup>-2</sup> d<sup>-1</sup> (Figure S1 in Supporting Information S1). These fluxes are low compared to other reported streams (Mulholland et al., 2001), with only the peak flux date of 3 December potentially influencing estimates of ER (R. O. Hall & Tank, 2005). We did not use this flux to correct our metabolism estimates both because of uncertainty in flux estimates due to our rating curves and unmeasured

CARTER ET AL. 9 of 17

21698961, 2022, 11, Do wnloaded from https://agupubs.onlinelibrary.wiley.com/doi/10.1029/2022/G007048 by University Of Wyoming Librarie, Wiley On line Library on [29/05/2023]. See the Terms

Significant relationships at  $p \le 0.01$ , 0.05, and 0.1 are indicated by \*\*\*, \*\*, and \*, respectively.

groundwater oxygen concentrations, but this analysis suggests that groundwater inputs were likely not important at the scale of this study.

The role of stream metabolism in shaping gas dynamics is reflected in the relationship between the molar departures of O<sub>2</sub> and CO<sub>2</sub> from atmospheric equilibrium (Figure 6a). Atmospheric exchange will tend to push both gases toward zero departure from equilibrium, and both in situ anaerobic metabolism and groundwater contributions

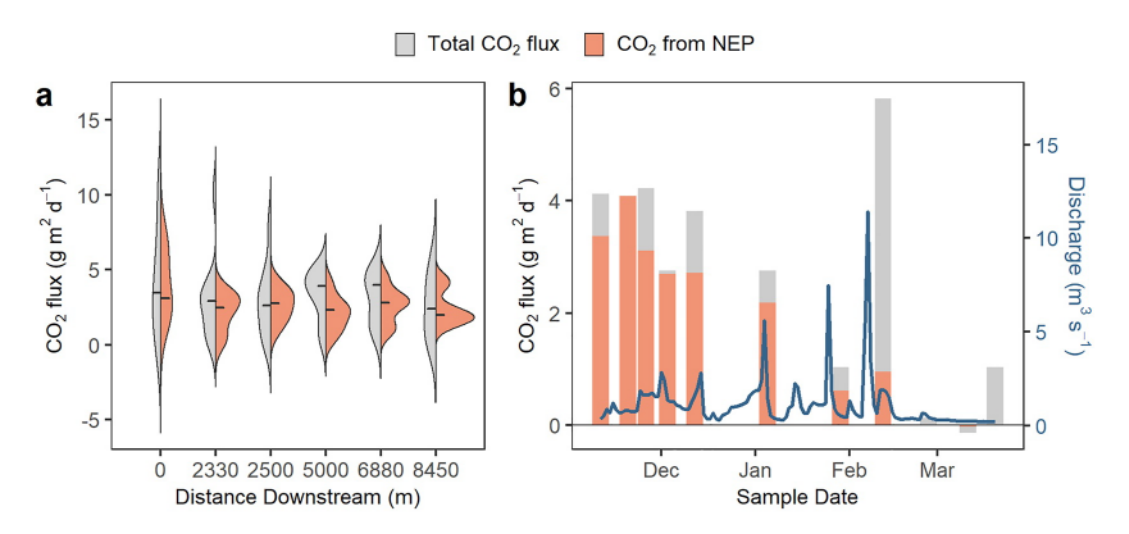


Figure 5. Almost all of the CO, flux is accounted for by in stream metabolism except on the falling limb of a large storm. (a) Gray distributions on the left show the range of CO2 fluxes across all dates which had positive flux at each site and orange distributions on the right show CO<sub>2</sub> generated by net ecosystem productivity (NEP) for those same days with a respiration quotient of 0.8. Distribution medians are indicated by horizontal lines. (b) Bars show total CO2 flux across sites on each sample date with the fraction attributable to NEP colored orange. Discharge at the outlet of the reach is shown on a linear scale in blue.

CARTER ET AL. 10 of 17

mlinelibrary.wiley.com/doi/10.1029/2022JG007048 by University Of Wyoming Librarie, Wiley Online Library on [29/05/2023]. See

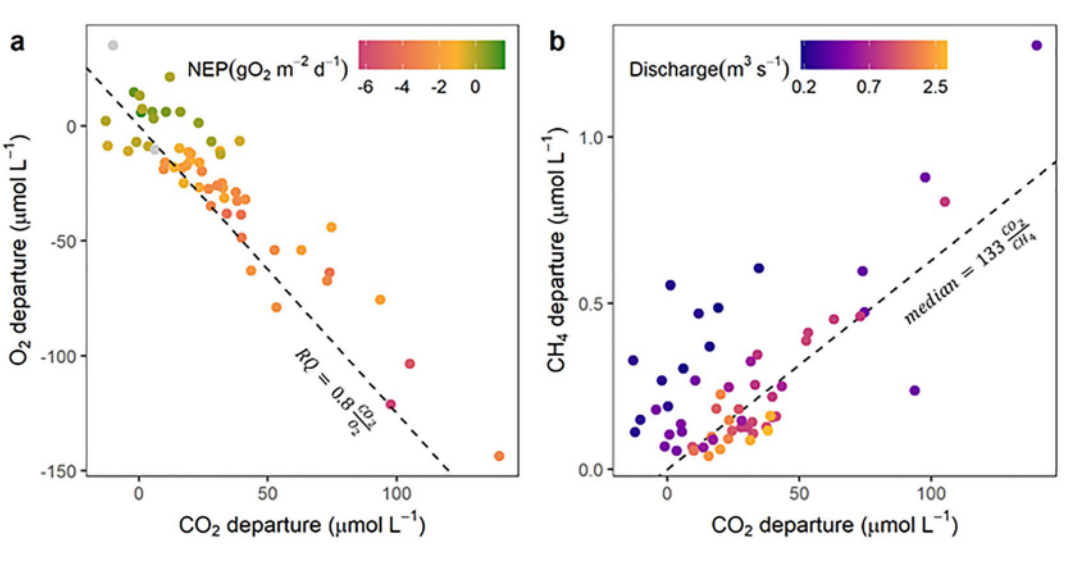


Figure 6. Ratios of excess gas concentrations across samples. (a) Dissolved  $CO_2$  and  $O_2$  in excess of the stream water saturation value for each gas sample. The line represents the pattern that would be expected in diel data corresponding with a respiratory quotient of 0.8 mol  $CO_2$  produced per mole  $O_2$ . The points are colored by net ecosystem productivity (GPP + ER). (b) Dissolved  $CH_4$  in excess of stream saturation plotted against excess  $CO_2$ . The data have a wide spread around a median molar ratio of 133 with purple indicating that samples with low discharge tend to be enriched in  $CH_4$  while yellow points show high discharge samples which are  $CH_4$  depleted relative to  $CO_2$ .

will typically increase  $\mathrm{CO}_2$  and decrease  $\mathrm{O}_2$  concentrations (Vachon et al., 2020). Across our samples,  $\mathrm{CO}_2$  and  $\mathrm{O}_2$  departures were negatively correlated and spanned a gradient from high  $\mathrm{O}_2$  and low  $\mathrm{CO}_2$  when the stream was autotrophic (NEP  $\sim 0.5$  g  $\mathrm{O}_2$  m<sup>-2</sup> d<sup>-1</sup>) to low  $\mathrm{O}_2$  and high  $\mathrm{CO}_2$  when the stream was heterotrophic (NEP  $\sim -6$  g  $\mathrm{O}_2$  m<sup>-2</sup> d<sup>-1</sup>). If in situ diel measurements of  $\mathrm{CO}_2$  and  $\mathrm{O}_2$  departures are largely driven by aerobic stream metabolism, we expect a negative relationship passing through the origin (Bernal et al., 2022; Vachon et al., 2020). Our samples were not diel, limiting this interpretation. However, if this relationship was primarily driven by groundwater, we would expect the entire relationship to move to the right, representing more  $\mathrm{CO}_2$  relative to  $\mathrm{O}_2$  depletion. Both the covariation of gas departures with NEP and the location of the relationship relative to the origin are consistent with stream metabolism as the dominant control, rather than groundwater inputs.

Concentrations of  $CH_4$  covaried with  $CO_2$  concentration with an average molar departure ratio of  $0.0031 \pm 0.15$ . The variance around this relationship is much higher than it is for  $O_2$  and  $CO_2$  and much of the spread around the line is related to stream discharge (Figure 6b). If these departures were primarily controlled by groundwater inputs and atmospheric exchange, we would expect high departures at low discharge and near zero departures at high discharge, which is not what we observe (Figure 6b). In general, samples taken at low discharge were enriched in  $CH_4$  relative to  $CO_2$  while those taken at high discharge were depleted. Much of this variation is seasonal; autumn and winter  $CH_4$ : $CO_2$  ratios average  $\sim 0.005$  with the lowest in early November and in the spring they increase to  $\sim 0.12$  with a few exceptionally high values. This increase overlaps with the spring productivity bloom and associated  $CO_2$  depletion which drives at least part of the shift. However,  $CH_4$  concentrations also increase in the spring, contributing to the shift.  $N_2O$  departures from saturation do not covary with any of the other gases.

### 4. Discussion

Over the course of this 5 month study, New Hope Creek was a net source of  $\mathrm{CO}_2$  and  $\mathrm{CH}_4$  to the atmosphere and a net sink of  $\mathrm{N}_2\mathrm{O}$  (Figure 2). Aerobic metabolism within the stream channel was the dominant driver of  $\mathrm{CO}_2$  dynamics and was likely important for  $\mathrm{CH}_4$  and  $\mathrm{N}_2\mathrm{O}$  as well. Seasonal variation in stream metabolism and hydrology drives most of the observed patterns in gas concentrations and fluxes. During late autumn, respiration fueled by the pulse of terrestrial litterfall was high, driving oxygen depletion, nitrate limitation, and  $\mathrm{CO}_2$  supersaturation. In the spring, algal photosynthesis led to a period of oxygen supersaturation and  $\mathrm{CO}_2$  depletion. Concentrations of  $\mathrm{CH}_4$  followed similar seasonal patterns as  $\mathrm{CO}_2$  with even larger magnitude shifts. Throughout the fall respiration

CARTER ET AL. 11 of 17

peak,  $N_2O$  concentrations were well below saturation, but both nitrate and  $N_2O$  concentrations increased in spring as the system moved toward autotrophy (Figure 3). This may indicate that  $N_2O$  production was limited by nitrate, depleted by heterotrophic bacteria in the fall. We suggest that the high predictability of GHG concentrations and fluxes by instream controls is a result of low hyporheic and atmospheric exchange, a claim supported by the low channel complexity and groundwater fluxes, flat stream gradients, and frequent large volume, high residence time pools in New Hope Creek.

#### 4.1. Magnitudes and Patterns

Concentrations of  $CO_2$  in New Hope Creek are comparable to those observed in similarly sized streams, but flux rates are much lower due to limited gas exchange. A synthesis of US streams reports an average  $CO_2$  concentration of 5.3 mg L<sup>-1</sup> [this study: 2.3; 0.2–7.1] (mean; range shown in brackets throughout section) and flux of 18.9 g m<sup>-2</sup> d<sup>-1</sup> [this study: 2.9; -0.4 to 10.5] in third order streams (Butman & Raymond, 2011). While the total flux from New Hope Creek is lower, the fraction of  $CO_2$  flux due to in stream metabolism is comparable to that in some streams (Bernal et al., 2022; Rocher-Ros et al., 2020) but higher than is reported in most streams of similar size (Gómez-Gener et al., 2016; Lupon et al., 2019; Rasilo et al., 2017). The fraction we measured is likely a conservative estimate, as we would expect the lowest contribution of instream metabolism during the winter, which is when we collected most of our measurements.

Methane (CH<sub>4</sub>) concentrations and fluxes are an order of magnitude lower than the average concentrations reported in a recent synthesis ( $22 \pm 83 \,\mu g \, L^{-1}$  [this study: 4.3; 0.7–20]) but are about equal to the mean of undisturbed reference streams ( $\sim 5 \,\mu g \, L^{-1}$ ) in the same synthesis (Stanley et al., 2016). Nitrous oxide (N<sub>2</sub>O) concentrations vary substantially across streams and rivers, and our concentrations are lower than most. This might be because many N<sub>2</sub>O studies are done in places where nitrate is high such as urban streams and agricultural streams, with average N<sub>2</sub>O about three times as high as in NHC ( $1.2 \,\mu g \, L^{-1}$ , Beaulieu et al., 2008) [this study: 0.5; 0–0.9], though a synthesis of forested streams found similarly high concentrations ( $1.3 \pm 1.8 \,\mu g \, L^{-1}$ , Audet et al., 2020). A synthesis from Quick et al. (2019) reports N<sub>2</sub>O fluxes ranging from -3 up to several thousand mg m<sup>-2</sup> d<sup>-1</sup> [this study: -0.2; -1.4–0.7]. While most studies in this synthesis show streams as a net source of N<sub>2</sub>O to the atmosphere, some, particularly in forested areas, report very low concentrations and occasional net absorption of N<sub>2</sub>O (e.g., -2 to 6 mg m<sup>-2</sup> d<sup>-1</sup>, Soued et al., 2016) as we observe at our site.

#### 4.2. Metabolism Controls

In-stream photosynthesis and aerobic respiration are directly responsible for the consumption and production of CO<sub>2</sub> in streams and explain a large fraction of variation in gas concentrations in New Hope Creek. On every date, the potential supply of DOC is more than sufficient to support the entire flux of CO<sub>2</sub> to the atmosphere based on typical DOC uptake rates (Mineau et al., 2016, Figure S7 in Supporting Information S1). Much of this water column DOC may not be labile, but large accumulations of POC in the streambed are also an important source of C to support heterotrophic metabolism as previously observed in New Hope Creek (Carter, 2021; C. A. S. Hall, 1972), and in other streams (Bertuzzo et al., 2022).

At times, net heterotrophic respiratory production of  $CO_2$  is much higher than the  $CO_2$  flux to the atmosphere, leading to an accumulation of  $CO_2$  in the stream, even when it is already supersaturated (Figure 5). This has been reported in arctic streams (Rocher-Ros et al., 2020), but has not been reported for low order streams like New Hope Creek which have previously been shown to derive the bulk of their  $CO_2$  flux to the atmosphere from groundwater inputs (Duvert et al., 2019; Hotchkiss et al., 2015; Rasilo et al., 2017). In part, this accumulation is due to a limited ability to exchange with the atmosphere. New Hope Creek is deep and slow moving, even in the winter months, and dissolved gas often remains in the water column for several days and in transit over multiple kilometers due to limited gas exchange. This can cause lags between gas production and degassing and creates ideal conditions for oxygen depletion driving the system hypoxic during periods of low flows and high temperatures (Carter et al., 2021).

While our metabolic rates do not incorporate measurements of anaerobic processes, they nonetheless serve as a strong predictor of  $CH_4$  concentration and flux. The "anaerobic scaling hypothesis" suggests that anaerobic respiration may increase proportionally to aerobic respiration, allowing  $CO_2$  or ER to serve as a predictor for  $CH_4$  concentrations (Stanley et al., 2016). This relationship can arise via two distinct but not mutually exclusive

CARTER ET AL. 12 of 17

mechanisms. First, aerobic respiration depletes oxygen, so periods of high aerobic respiration can lead to oxygen depletion which favors anaerobic methanogenesis while low respiration may sustain high oxygen concentrations which can facilitate CH<sub>4</sub> oxidation in the water column (Stanley et al., 2016). An alternative mechanisms is that both aerobic respiration and CH<sub>4</sub> production are stimulated whenever there are large allochthonous organic matter subsidies such as terrestrial litterfall (Roberts et al., 2007) or DOC pulses from storm flows (Demars, 2019).

Even when the stream water column is well oxygenated, measurable CH<sub>4</sub> concentrations and fluxes are present, indicating the potential for respiration at all levels on the redox ladder to be co-occurring throughout the sediments or in the water column (Bogard et al., 2014; Megonigal et al., 2004). When respiration increases, so does the CH<sub>4</sub>:CO<sub>2</sub> ratio (Figure 3), meaning that the fraction of respiration occurring through CH<sub>4</sub> producing pathways is increasing. This might indicate that electron acceptors are more limiting than organic carbon in anoxic microsites and CH<sub>4</sub> production proceeds in the absence of more energetically favorable electron acceptors (Megonigal et al., 2004). Indeed, the sediments contain large amounts of buried organic carbon, and storms frequently replenish DOC in the water column (Zimmer & McGlynn, 2018).

In New Hope Creek, the anaerobic scaling hypothesis did not extend to  $N_2O$ , an intermediate product of both anaerobic (denitrification) and aerobic (nitrification) metabolic pathways (Quick et al., 2019). Some studies have found that increased respiration predicts  $N_2O$  fluxes from streams (Beaulieu et al., 2011; Madinger & Hall, 2019; Reisinger et al., 2016). This relationship may arise when high organic matter availability drives both aerobic respiration and denitrification, or if respiratory demand depletes oxygen, favoring the use of nitrate as an alternative electron acceptor to fuel anaerobic respiration via denitrification (Rosamond et al., 2012). In New Hope Creek, we do see a slight increase in  $N_2O$  fluxes with lower oxygen, but this relationship is not strong. Instead, in New Hope Creek, fluxes of  $N_2O$  between the stream and atmosphere shift from outgassing when respiration is low to net influx at times of high respiration (Figure 3). In fact, the stream was a net sink of  $N_2O$  during the autumn respiration peak, though, even on the date with the highest rate of  $N_2O$  absorption, this offsets only 8% of the total flux of GHGs in  $CO_2$  equivalents (Figure S8 in Supporting Information S1).

Throughout the autumn, nitrate appears to be limiting  $N_2O$  production as denitrifiers are potentially out-competed by aerobic heterotrophs during the respiration peak. In the winter and spring, nitrate demand drops in the absence of large terrestrial organic matter subsidies and  $N_2O$  concentrations and fluxes slowly catch up and remain high through the spring (Figure 3). Nitrogen is not limiting in the spring in New Hope Creek (Covino et al., 2018), and denitrifiers are able to coexist with autotrophs. Additionally, the response of  $CH_4$  production to increased respiration is not as strong in the spring as in the autumn. One possible explanation of this is that  $CH_4$  production is reduced by greater availability of  $NO_3$ , which is a more energetically favorable electron acceptor than organic carbon (Megonigal et al., 2004).

# 4.3. Physical Controls

In stream physical drivers are also important in predicting gas dynamics. Concentrations of  $CO_2$  were consistently lower during periods of warmer water temperatures. This result is somewhat counterintuitive given the well documented increases in metabolic rates with temperature (Yvon-Durocher et al., 2012; Zhu et al., 2020) but can be explained because the high energy input to the stream via litterfall occurs during the late autumn when temperatures are colder (Valett et al., 2008). Though substrate supply overrides any effect of temperature on metabolic  $CO_2$  production, warmer temperatures do reduce the solubility of GHG, contributing to enhanced degassing. In combination reduced solubility and reduced substrate supply lead to lower  $CO_2$  concentrations in warmer months.

Long water residence times may favor anaerobic metabolism (Gomez-Gener et al., 2020). We see a distinct shift toward higher  $\mathrm{CH_4:CO_2}$  ratios with lower discharge in New Hope Creek (Figure 6). An increase in anaerobic processes with low discharge may be attributed to higher groundwater exchange or porewater seepage (Taillardat et al., 2022), the development of anoxic regions within the channel, or less atmospheric exchange. Geomorphologies that have consistently low water velocities such as pools tend to accumulate fine sediments that settle out of the water column, creating conditions conducive to sediment hypoxia (Stanley et al., 2016). All these factors suggest there would be a greater accumulation of metabolic byproducts at low discharge, and it is likely that with longer residence times, a greater proportion of those byproducts will be from lower on the redox ladder.

Storm flows shift the controls on gas flux away from instream production in favor of terrestrial inputs. The only sampling date where less than half of the  $CO_2$  flux was derived from instream production was on the falling limb

CARTER ET AL. 13 of 17

of a large storm (Figure 5). This could be explained by large amounts of terrestrial  $CO_2$  entering in from ground-water during the storm (Jones & Mulholland, 1998) or by the opportunistic venting of a large quantity of  $CO_2$  that had accumulated in the stream, trapped by low gas exchange. This suggests that while instream controls dominate in New Hope Creek on average, storms may serve as temporal control points when infrequent but large inputs of inorganic carbon control the budget.

#### 4.4. Spatial Controls

Although most of the variation in gases in New Hope Creek was seasonal, we did observe consistent spatial patterns across sampling dates (Figure 2). This variation appears to be related to channel structure, with flatter segments with longer water residence times characterized by lower oxygen concentrations and the accumulation of more respiration byproducts. CH<sub>4</sub> is more linked to local variability than the other gases, and there were consistent control points where CH<sub>4</sub> concentrations were higher, suggesting production from anaerobic metabolism or input from groundwater. The spatial variability in all gases was the highest in the autumn respiration peak; a low flow time when the stream was likely to be losing water (Zimmer & McGlynn, 2017) which would result in minimal groundwater inputs and less mixing with the hyporheic zone (Fox et al., 2014), conditions which favor anaerobic metabolic pathways.

In New Hope Creek, small, often steep, bedrock riffles separate the large pools and create points of turbulent mixing, even at low flows. They serve as control points for gas evasion, especially in this low gradient stream where gas exchange coefficients are universally low elsewhere. These exert strong control on gas evasion and consistently move gases toward equilibrium with the atmosphere in all seasons (Rocher-Ros et al., 2019).

#### 5. Conclusions

Very few individual research studies have collected sufficiently comprehensive data sets to estimate annual GHG fluxes from rivers, still fewer have collected concomitant data to enable researchers to estimate groundwater GHG contributions or stream respiration rates at the same time. The lack of such information currently significantly limits our ability to measure or model how riverine contributions to the global carbon cycle are changing in response to the rising temperatures, altered hydrology, and enhanced organic matter and nutrient loads that characterize most rivers of the Anthropocene. GHG fluxes out of New Hope Creek are low relative to ranges reported in the literature (Quick et al., 2019; Raymond et al., 2013; Stanley et al., 2016). Long water residence times, low groundwater inputs, and limited reaeration create ideal conditions for instream metabolic processes to drive GHG concentrations and fluxes. At times, instream photosynthesis is high enough to deplete stream CO<sub>2</sub> below saturation and during periods of peak heterotrophic respiration the river becomes a net sink for N<sub>2</sub>O. Seasonal variation in instream GPP and ER that drives the temporal variation in GHGs observed throughout New Hope Creek. We also see consistent differences between river segments linked to channel geomorphology. River segments with the longest water residence times store substantial quantities of organic matter and are primary sources of respiratory products (Casas-Ruiz et al., 2017; Gómez-Gener et al., 2015), while rare high velocity sections act as the control points at which the majority of GHGs are vented to the atmosphere (Rocher-Ros et al., 2019). Our results suggest that organic matter inputs and storage along with nutrient limitation determine the timing and magnitude of gas production while hydrologic regimes and hydraulic gradients constrain these rates and determine the balance between instream controls and external sources. Our study in New Hope Creek provides an important counterexample to the dominant assumption that terrestrial contributions dominate riverine GHG emissions (Duvert et al., 2018). While certainly true at the global scale, this assumption may be highly inaccurate for many regions. The geomorphic conditions and human modifications that lead to high organic matter and water residence times in New Hope Creek are not unique (Wohl & Merritts, 2007), we suspect that similar instream controls on riverine GHG emissions will be observed in low gradient headwater streams throughout the world.

# **Data Availability Statement**

The greenhouse gas data and all covariates used for this manuscript and the code used to complete all analyses and generate the figures are available at zenodo via <a href="https://doi.org/10.5281/zenodo.7240419">https://doi.org/10.5281/zenodo.7240419</a> (Carter, 2022) with a GPL 3.0 license.

CARTER ET AL. 14 of 17



# Journal of Geophysical Research: Biogeosciences

10.1029/2022JG007048

#### Acknowledgments

This research was done on the ancestral lands of the Haliwa-Saponi, Sappony, and Occaneechi-Saponi nations. The authors thank Brooke Hassett, Alexander Miele, Cathy Chamberlin, Johnny Behrens, Wyatt Jernigan, and Emily Ury for assistance with field and laboratory work and Ashley Helton, Robert Hall, Jim Heffernan, and Martin Doyle for conceptual development and helpful comments on a draft of this manuscript. Funding for this work was from the NSF Macrosystems Biology Award 1442439 and EPSCoR RII Track-2 FEC Award 2019528.

#### References

- Appling, A. P., Hall, R. O., Arroita, M., & Yackulic, C. B. (2018). streamMetabolizer: Models for estimating aquatic photosynthesis and respiration. R package. (Version 0.10.9). Retrieved from https://github.com/USGS-R/streamMetabolizer
- Appling, A. P., Hall, R. O., Yackulic, C. B., & Arroita, M. (2018). Overcoming equifinality: Leveraging long time series for stream metabolism estimation. *Journal of Geophysical Research: Biogeosciences*, 123(2), 624–645. https://doi.org/10.1002/2017JG004140
- Audet, J., Bastviken, D., Bundschuh, M., Buffam, I., Feckler, A., Klemedtsson, L., et al. (2020). Forest streams are important sources for nitrous oxide emissions. Global Change Biology, 26(2), 629–641. https://doi.org/10.1111/gcb.14812
- Aufdenkampe, A. K., Mayorga, E., Raymond, P. A., Melack, J. M., Doney, S. C., Alin, S. R., et al. (2011). Riverine coupling of biogeochemical cycles between land, oceans, and atmosphere. Frontiers in Ecology and the Environment, 9(1), 53–60. https://doi.org/10.1890/100014
- Bates, D., Mächler, M., Bolker, B. M., & Walker, S. C. (2015). Fitting linear mixed-effects models using lme4. *Journal of Statistical Software*, 67(1), 1–18. https://doi.org/10.18637/jss.v067.i01
- Battin, T. J., Luyssaert, S., Kaplan, L. A., Aufdenkampe, A. K., Richter, A., & Tranvik, L. J. (2009). The boundless carbon cycle. *Nature Geoscience*, 2(9), 598–600. https://doi.org/10.1038/ngeo618
- Beaulieu, J. J., Arango, C. P., Hamilton, S. K., & Tank, J. L. (2008). The production and emission of nitrous oxide from headwater streams in the Midwestern United States. Global Change Biology, 14(4), 878–894. https://doi.org/10.1111/j.1365-2486.2007.01485.x
- Beaulieu, J. J., Tank, J. L., Hamilton, S. K., Wollheim, W. M., Hall, R. O., Mulholland, P. J., et al. (2011). Nitrous oxide emission from denitrification in stream and river networks. Proceedings of the National Academy of Sciences of the United States of America, 108(1), 214–219. https://doi.org/10.1073/pnas.1011464108
- Beier, P., Burnham, K. P., & Anderson, D. R. (2001). Model selection and inference: A practical information-theoretic approach. *Journal of Wildlife Management*, 65(3), 606. https://doi.org/10.2307/3803117
- Bernal, S., Cohen, M. J., Ledesma, J. L. J., Kirk, L., Martí, E., & Lupon, A. (2022). Stream metabolism sources a large fraction of carbon dioxide to the atmosphere in two hydrologically contrasting headwater streams. *Limnology & Oceanography*, 9999, 1–14. https://doi.org/10.1002/ lno.12226
- Bernhardt, E. S., Blaszczak, J. R., Ficken, C. D., Fork, M. L., Kaiser, K. E., & Seybold, E. C. (2017). Control points in ecosystems: Moving beyond the hot spot hot moment concept. *Ecosystems*, 20(4), 665–682. https://doi.org/10.1007/s10021-016-0103-y
- Bernhardt, E. S., Savoy, P., Vlah, M. J., Appling, A. P., Koenig, L. E., Jr, R. O. H., et al. (2022). Light and flow regimes regulate the metabolism of rivers. *Proceedings of the National Academy of Sciences*, 119(8), 5. https://doi.org/10.1073/pnas.2121976119
- Bertuzzo, E., Hotchkiss, E. R., Argerich, A., Kominoski, J. S., Oviedo-Vargas, D., Savoy, P., et al. (2022). Respiration regimes in rivers: Partitioning source-specific respiration from metabolism time series. *Limnology & Oceanography*, 9999, 1–15. https://doi.org/10.1002/lno.12207
- Blackburn, S. R., & Stanley, E. H. (2021). Floods increase carbon dioxide and methane fluxes in agricultural streams. Freshwater Biology, 66(1), 62–77. https://doi.org/10.1111/fwb.13614
- Blaszczak, J. R., Delesantro, J. M., Urban, D. L., Doyle, M. W., & Bernhardt, E. S. (2019). Scoured or suffocated: Urban stream ecosystems oscillate between hydrologic and dissolved oxygen extremes. *Limnology & Oceanography*, 64(3), 877–894. https://doi.org/10.1002/lno.11081 Blodgett, D. (2019). nhdplusTools: Tools for accessing and working with the NHDPlus, version 0.3.8. Retrieved from https://code.usgs.gov/water/nhdplusTools
- Bogard, M. J., del Giorgio, P. A., Boutet, L., Chaves, M. C. G., Prairie, Y. T., Merante, A., & Derry, A. M. (2014). Oxic water column methanogenesis as a major component of aquatic CH<sub>4</sub> fluxes. *Nature Communications*, 5(1), 5350. https://doi.org/10.1038/ncomms6350
- Butman, D., & Raymond, P. A. (2011). Significant efflux of carbon dioxide from streams and rivers in the United States. *Nature Geoscience*, 4(12), 839–842. https://doi.org/10.1038/ngeo1294
- Carter, A. M. (2021). Shifting thermal and metabolic regimes in a low gradient, temperate river network (Dissertation). Duke University. Retrieved from https://hdl.handle.net/10161/23088
- Carter, A. M. (2022). amcarter/GHG: GHG processing code v1.1 (v1.1). Zenodo. https://doi.org/10.5281/zenodo.7240419
- Carter, A. M., Blaszczak, J. R., Heffernan, J. B., & Bernhardt, E. S. (2021). Hypoxia dynamics and spatial distribution in a low gradient river. Limnology & Oceanography, 66(6), 2251–2265. https://doi.org/10.1002/lno.11751
- Casas-Ruiz, J. P., Catalán, N., Gómez-Gener, L., von Schiller, D., Obrador, B., Kothawala, D. N., et al. (2017). A tale of pipes and reactors: Controls on the in-stream dynamics of dissolved organic matter in rivers. *Limnology & Oceanography*, 62(S1), S85–S94. https://doi.org/10.1002/jno.10471
- Catalán, N., Marcé, R., Kothawala, D. N., & Tranvik, L. J. (2016). Organic carbon decomposition rates controlled by water retention time across inland waters. Nature Geoscience, 9(7), 501–504. https://doi.org/10.1038/ngeo2720
- Chapra, S. C., & Di Toro, D. M. (1991). Delta method for estimating primary production, respiration, and reaeration in streams. *Journal of Environmental Engineering*, 117(5), 640–655. https://doi.org/10.1061/(asce)0733-9372(1991)117:5(640)
- Cole, J., Prairie, Y. T., Caraco, N. F., McDowell, W. H., Tranvik, L. J., Striegl, R. G., et al. (2007). Plumbing the global carbon cycle: Integrating inland waters into the terrestrial carbon budget. *Ecosystems*, 10(1), 171–184. https://doi.org/10.1007/s10021-006-9013-8
- Cole, J. J., Caraco, N. F., & Caraco, N. F. (2001). Carbon in catchments: Connecting terrestrial carbon losses with aquatic metabolism. Marine and Freshwater Research, 52(1), 101–110. https://doi.org/10.1071/MF00084
- Covino, T. P., Bernhardt, E. S., & Heffernan, J. B. (2018). Measuring and interpreting relationships between nutrient supply, demand, and limitation. Freshwater Science, 37(3), 448–455. https://doi.org/10.1086/699202
- Crawford, J. T., Lottig, N. R., Stanley, E. H., Walker, J. F., Hanson, P. C., Finlay, J. C., & Striegl, R. G. (2014). CO<sub>2</sub> and CH<sub>4</sub> emissions from streams in a lake-rich landscape: Patterns, controls, and regional significance. Global Biogeochemical Cycles, 28(3), 197–210. https://doi.org/10.1002/2013GB004661
- Crawford, J. T., Striegl, R. G., Wickland, K. P., Dornblaser, M. M., & Stanley, E. H. (2013). Emissions of carbon dioxide and methane from a headwater stream network of interior Alaska. *Journal of Geophysical Research: Biogeosciences*, 118(2), 482–494. https://doi.org/10.1002/ jgrg.20034
- del Giorgio, P. A., & Peters, R. H. (1994). Patterns in planktonic P:R ratios in lakes: Influence of lake trophy and dissolved organic carbon. Limnology & Oceanography, 39(4), 772–787. https://doi.org/10.4319/lo.1994.39.4.0772
- Demars, B. O. L. (2019). Hydrological pulses and burning of dissolved organic carbon by stream respiration. *Limnology & Oceanography*, 64(1), 406–421. https://doi.org/10.1002/lno.11048
- Demars, B. O. L., Gíslason, G. M., Ólafsson, J. S., Manson, J. R., Friberg, N., Hood, J. M., et al. (2016). Impact of warming on CO<sub>2</sub> emissions from streams countered by aquatic photosynthesis. *Nature Geoscience*, 9(10), 758–761. https://doi.org/10.1038/ngeo2807

CARTER ET AL. 15 of 17

21698961

- Duvert, C., Bossa, M., Tyler, K. J., Wynn, J. G., Munksgaard, N. C., Bird, M. I., et al. (2019). Groundwater-derived DIC and carbonate buffering enhance fluvial CO<sub>2</sub> evasion in two Australian tropical rivers. *Journal of Geophysical Research: Biogeosciences*, 124(2), 312–327. https://doi. org/10.1029/2018JG004912
- Duvert, C., Butman, D. E., Marx, A., Ribolzi, O., & Hutley, L. B. (2018). CO<sub>2</sub> evasion along streams driven by groundwater inputs and geomorphic controls. *Nature Geoscience*, 11(11), 813–818. https://doi.org/10.1038/s41561-018-0245-y
- Fox, A., Boano, F., & Arnon, S. (2014). Impact of losing and gaining streamflow conditions on hyporheic exchange fluxes induced by dune-shaped bed forms. Water Resources Research, 50(3), 1895–1907. https://doi.org/10.1002/2013WR014668
- Gomez-Gener, L., Lupon, A., Laudon, H., & Sponseller, R. A. (2020). Drought alters the biogeochemistry of boreal stream networks. Nature Communications, 11(1), 1795. https://doi.org/10.1038/s41467-020-15496-2
- Gómez-Gener, L., Obrador, B., von Schiller, D., Marcé, R., Casas-Ruiz, J. P., Proia, L., et al. (2015). Hot spots for carbon emissions from Mediterranean fluvial networks during summer drought. Biogeochemistry, 125(3), 409–426. https://doi.org/10.1007/s10533-015-0139-7
- Gómez-Gener, L., von Schiller, D., Marcé, R., Arroita, M., Casas-Ruiz, J. P., Staehr, P. A., et al. (2016). Low contribution of internal metabolism to carbon dioxide emissions along lotic and lentic environments of a Mediterranean fluvial network. *Journal of Geophysical Research: Biogeosciences*, 121(12), 3030–3044. https://doi.org/10.1002/2016JG003549
- Goodman, K. (2021). AOS protocol and procedure: SDG Surface water dissolved gas sampling (No. NEON.DOC.001199, p. 50). National Ecological Observatory Network.
- Hall, C. A. S. (1972). Migration and metabolism in a temperate stream ecosystem. Ecology, 53(4), 585-604. https://doi.org/10.2307/1934773
- Hall, R. O., & Ulseth, A. J. (2020). Gas exchange in streams and rivers. WIREs Water, 7(1), 1–18. https://doi.org/10.1002/wat2.1391 Hall, R. O., & Madinger, H. L. (2018). Use of argon to measure gas exchange in turbulent mountain streams. Biogeosciences, 15(10), 3085–3092.
- Hall, R. O., & Madinger, H. L. (2018). Use of argon to measure gas exchange in turbulent mountain streams. *Biogeosciences*, 15(10), 3085–3092 https://doi.org/10.5194/bg-15-3085-2018
- Hall, R. O., & Tank, J. L. (2005). Correcting whole-stream estimates of metabolism for groundwater input. Limnology and Oceanography: Methods, 3(4), 222–229. https://doi.org/10.4319/lom.2005.3.222
- Holgerson, M. A., & Raymond, P. A. (2016). Large contribution to inland water CO<sub>2</sub> and CH<sub>4</sub> emissions from very small ponds. *Nature Geoscience*, 9(3), 222–226. https://doi.org/10.1038/ngeo2654
- Hotchkiss, E. R., Hall, R. O., Jr., Sponseller, R. A., Butman, D., Klaminder, J., Laudon, H., et al. (2015). Sources of and processes controlling CO<sub>2</sub> emissions change with the size of streams and rivers. *Nature Geoscience*, 8(9), 696–699. https://doi.org/10.1038/ngeo2507
- Hudson, F. (2004). Sample preparation and calculations for dissolved gas analysis in water samples using a GC headspace equilibration technique (RSKSOP-175). U.S. EPA.
- Hurvich, C. M., & Tsai, C. L. (1989). Regression and time series model selection in small samples. Biometrika, 76(2), 297–307. https://doi.org/10.1093/biomet/76.2.297
- Jones, J. B., & Mulholland, P. J. (1998). Influence of drainage basin topography and elevation on carbon dioxide and methane supersaturation of stream water. *Biogeochemistry*, 40(1), 57–72. https://doi.org/10.1023/A;1005914121280
- Junker, J. R., Cross, W. F., Benstead, J. P., Huryn, A. D., Hood, J. M., Nelson, D., et al. (2020). Flow is more important than temperature in driving patterns of organic matter storage and stoichiometry in stream ecosystems. *Ecosystems*, 24(6), 1317–1331. https://doi.org/10.1007/
- s10021-020-00585-6
  Leach, J. A., Lidberg, W., Kuglerová, L., Peralta-Tapia, A., Ågren, A., & Laudon, H. (2017). Evaluating topography-based predictions of shallow lateral groundwater discharge zones for a boreal lake-stream system. Water Resources Research, 53(7), 5420-5437. https://doi.
- org/10.1002/2016WR019804
  Leopold, L. B., & Maddock, T., Jr. (1953). The hydraulic geometry of stream channels and some physiographic implications (Report No. 252),
- Professional Paper. U.S. Government Printing Office. https://doi.org/10.3133/pp252

  Li, M., Peng, C., Zhang, K., Xu, L., Wang, J., Yang, Y., et al. (2021). Headwater stream ecosystem: An important source of greenhouse gases to the atmosphere. Water Research, 190, 116738. https://doi.org/10.1016/j.watres.2020.116738
- Lindsay, J. B. (2014). The whitebox geospatial analysis tools project and open-access GIS. In Proceedings of the GIS Research UK 22nd Annual Conference. The University of Glasgow. https://doi.org/10.13140/RG.2.1.1010.8962
- Lupon, A., Denfeld, B. A., Laudon, H., Leach, J., Karlsson, J., & Sponseller, R. A. (2019). Groundwater inflows control patterns and sources of greenhouse gas emissions from streams. Limnology & Oceanography, 64(4), 1545–1557. https://doi.org/10.1002/lno.11134
- Madinger, H. L., & Hall, R. O. (2019). Linking denitrification with ecosystem respiration in mountain streams. Limnology and Oceanography Letters, 4(5), 145–154. https://doi.org/10.1002/jol2.10111
- Megonigal, J. P., Hines, M. E., & Visscher, P. T. (2004). Anaerobic metabolism: Linkages to trace gases and aerobic processes. In W. H. Schlesinger (Ed.), *Biogeochemistry* (pp. 317–424). Elsevier Pergamon. https://doi.org/10.1016/B0-08-043751-6/08132-9
- Mineau, M. M., Wollheim, W. M., Buffam, I., Findlay, S. E. G., Hall, R. O., Hotchkiss, E., et al. (2016). Dissolved organic carbon uptake in streams:

  A review and assessment of reach-scale measurements. Limnology & Oceanography, 121(8), 1–11. https://doi.org/10.1002/2015JG003204
- Mulholland, P. J., Fellows, C. S., Hamilton, S. K., Marti, E., Division, E. S., Ridge, O., et al. (2001). Inter-biome comparison of factors controlling stream metabolism. Freshwater Biology, 46(11), 1503–1517. https://doi.org/10.1046/j.1365-2427.2001.00773.x
- Nakagawa, S., & Schielzeth, H. (2013). A general and simple method for obtaining R<sup>2</sup> from generalized linear mixed-effects models. *Methods in Ecology and Evolution*, 4(2), 133–142. https://doi.org/10.1111/j.2041-210x.2012.00261.x
- Quick, A. M., Benner, S. G., Reeder, W. J., Farrell, T. B., Tonina, D., & Feris, K. P. (2019). Nitrous oxide from streams and rivers: A review of primary biogeochemical pathways and environmental variables. *Earth-Science Reviews*, 191, 224–262. https://doi.org/10.1016/j.earscirev.2019.02.021
- Rasilo, T., Hutchins, R. H. S., Ruiz-González, C., & del Giorgio, P. A. (2017). Transport and transformation of soil-derived CO<sub>2</sub>, CH<sub>4</sub> and DOC sustain CO<sub>2</sub> supersaturation in small boreal streams. Science of the Total Environment, 579, 902–912. https://doi.org/10.1016/j.scitotenv.2016.10.187
- Raymond, P. A., Hartmann, J., Lauerwald, R., Sobek, S., McDonald, C., Hoover, M., et al. (2013). Global carbon dioxide emissions from inland waters. *Nature*, 503(7476), 355–359. https://doi.org/10.1038/nature12760
- Raymond, P. A., Zappa, C. J., Butman, D., Bott, T. L., Potter, J., Mulholland, P., et al. (2012). Scaling the gas transfer velocity and hydraulic geometry in streams and small rivers. Limnology and Oceanography: Fluids and Environments, 2(1), 41–53. https://doi.org/10.1215/21573689-1597669
- R Core Team. (2022). R: A language and environment for statistical computing. R Foundation for Statistical Computing. Retrieved from https://www.R-project.org/
- Reisinger, A. J., Tank, J. L., Hoellein, T. J., & Hall, R. O. (2016). Sediment, water column, and open-channel denitrification in rivers measured using membrane-inlet mass spectrometry. *Journal of Geophysical Research: Biogeosciences*, 121(5), 1258–1274. https://doi.org/10.1002/2015JG003261.Received

CARTER ET AL. 16 of 17

- Roberts, B. J., Mulholland, P. J., & Hill, W. R. (2007). Multiple scales of temporal variability in ecosystem metabolism rates: Results from 2 years of continuous monitoring in a forested headwater stream. *Ecosystems*, 10(4), 588–606. https://doi.org/10.1007/s10021-007-9059-2
- Rocher-Ros, G., Sponseller, R. A., Bergström, A. K., Myrstener, M., & Giesler, R. (2020). Stream metabolism controls diel patterns and evasion of CO<sub>2</sub> in Arctic streams. Global Change Biology, 26(3), 1400–1413. https://doi.org/10.1111/gcb.14895
- Rocher-Ros, G., Sponseller, R. A., Lidberg, W., Mörth, C., & Giesler, R. (2019). Landscape process domains drive patterns of CO<sub>2</sub> evasion from river networks. *Limnology and Oceanography Letters*, 4(4), 87–95. https://doi.org/10.1002/loi2.10108
- Rosamond, M. S., Thuss, S. J., & Schiff, S. L. (2012). Dependence of riverine nitrous oxide emissions on dissolved oxygen levels. Nature Geoscience, 5(10), 715–718. https://doi.org/10.1038/ngeo1556
- Schade, J. D., Bailio, J., & McDowell, W. H. (2016). Greenhouse gas flux from headwater streams in New Hampshire, USA: Patterns and drivers. Limnology & Oceanography, 61(S1), S165–S174. https://doi.org/10.1002/lno.10337
- Soued, C., Giorgio, P. A., & Maranger, R. (2016). Nitrous oxide sinks and emissions in boreal aquatic networks in. *Québec*, 9, 116–120. https://doi.org/10.1038/NGEO2611
- Stanley, E. H., Casson, N. J., Christel, S. T., Crawford, J. T., Loken, L. C., & Oliver, S. K. (2016). The ecology of methane in streams and rivers: Patterns, controls, and global significance. *Ecological Monographs*, 86(2), 146–171. https://doi.org/10.1890/15-1027
- Taillardat, P., Bodmer, P., Deblois, C. P., Ponçot, A., Prijac, A., Riahi, K., et al. (2022). Carbon dioxide and methane dynamics in a peatland headwater stream: Origins, processes and implications. *Journal of Geophysical Research: Biogeosciences*, 127(7), e2022JG006855. https://doi.org/10.1029/2022JG006855
- Taylor, R. G., Scanlon, B., Döll, P., Rodell, M., van Beek, R., Wada, Y., et al. (2013). Ground water and climate change. *Nature Climate Change*, 3(4), 322–329. https://doi.org/10.1038/nclimate1744
- U.S. Geological Survey. (2017). National Hydrography Dataset Plus High Resolution (NHDPlus HR). Retrieved from https://www.usgs.gov/national-hydrography/hhdplus-high-resolution
- Vachon, D., Sadro, S., Bogard, M. J., Lapierre, J., Baulch, H. M., Rusak, J. A., et al. (2020). Paired O<sub>2</sub>–CO<sub>2</sub> measurements provide emergent insights into aquatic ecosystem function. *Limnology and Oceanography Letters*, 5(4), 287–294. https://doi.org/10.1002/lol2.10135
- Valett, H. M., Thomas, S. A., Mulholland, P. J., Webster, J. R., Dahm, C. N., Fellows, C. S., et al. (2008). Endogenous and Exogenous control of ecosystem function: N cycling in headwater streams. *Ecology*, 89(12), 3515–3527. https://doi.org/10.1890/07-1003.1
- Vannote, R. L., Minshall, W. G., Cummins, K. W., Sedell, J. R., & Cushing, C. E. (1980). The river continuum concept. Canadian Journal of Fisheries and Aquatic Sciences, 37(1), 130–137. https://doi.org/10.1139/f80-017
- Wohl, E., & Merritts, D.J. (2007). What is a natural river? Geography Compass, I(4), 871–900. https://doi.org/10.1111/j.1749-8198.2007.00049.x Yvon-Durocher, G., Allen, A. P., Bastviken, D., Conrad, R., Gudasz, C., St-Pierre, A., et al. (2014). Methane fluxes show consistent temperature
- dependence across microbial to ecosystem scales. *Nature*, 507(7493), 488–491. https://doi.org/10.1038/nature13164

  Yvon-Durocher, G., Caffrey, J. M., Cescatti, A., Dossena, M., Giorgio, P. D., Gasol, J. M., et al. (2012). Reconciling the temperature dependence
- of respiration across timescales and ecosystem types. *Nature*, 487(7408), 472–476. https://doi.org/10.1038/nature11205
- Yvon-Durocher, G., Jones, J. I., Trimmer, M., Woodward, G., & Montoya, J. M. (2010). Warming alters the metabolic balance of ecosystems. Philosophical Transactions of the Royal Society B: Biological Sciences, 365(1549), 2117–2126. https://doi.org/10.1098/rstb.2010.0038
- Zhu, Y., Purdy, K. J., Eyice, Ö., Shen, L., Harpenslager, S. F., Yvon-Durocher, G., et al. (2020). Disproportionate increase in freshwater methane emissions induced by experimental warming. *Nature Climate Change*, 10(7), 685–690. https://doi.org/10.1038/s41558-020-0824-y
- Zimmer, M. A., & McGlynn, B. L. (2017). Bidirectional stream-groundwater flow in response to ephemeral and intermittent streamflow and groundwater seasonality. Hydrological Processes, 31(22), 3871–3880. https://doi.org/10.1002/hyp.11301
- Zimmer, M. A., & McGlynn, B. L. (2018). Lateral, vertical, and longitudinal source area connectivity drive runoff and carbon Export across watershed scales. Water Resources Research, 54(3), 1576–1598. https://doi.org/10.1002/2017WR021718

CARTER ET AL. 17 of 17